Preface

The thesis that lies in front of you at this particular moment, completes my education at Hasselt University & KU Leuven. Instead of considering this the final closure of a memorable student period, this work marks to me the beginning of a new and exciting adventure lying of in front of me. Nevertheless I am very much looking forward to this new start, I also would like to make use of this opportunity to reflect and thank the people that contributed to this work.

First and foremost I would like to thank Prof. Johan Auwerx for giving me the chance to execute my final project in his lab. Being a part of top-notch research has been a very enriching experience, both personally and professionally.

Also I warmly thank my international coordinator Greet Raymaekers for setting up this new international collaboration with Prof. Auwerx. Hopefully many other students after me will make use of this exceptional opportunity.

I am very grateful to my supervisor, Dr. Norman Moullan, who invested a lot of time and effort in teaching me, advising me and supporting me during good and bad times. He gave me the insight to always try to perform beyond the average achievement.

Furthermore, many thanks to Thibaud Clerc, who taught me and provided us his great LC-MS/MS troubleshooting skills.

Thanks also to Dr. Pooja Jha for giving regularly her input to this project and the correction of this report.

I would also like to thank all members of the NCEM and UPSCHOONJANS lab that contributed to this work and in general, to my entire stay.

Outside of this laboratory, I want to thank my internal promotor Dr. ir. Kristel for the thesis revision.

And last but not least I owe many thanks to my parents, for supporting me during my study and encouraging me to pursue my international dream.

Table of Content

List of tables

List of figures

Abbreviations

ADP	Adenosine diphosphate
AMPK	AMP-activated protein kinase
ATP	Adenosine triphosphate
BAT	Brown adipose tissue
BSA	Bovine Serum Albumin
cADP	Cyclic ADP ribose synthetases
CD	Chow diet
CV	Coefficient of variation
ETC	Electron transport chain
FA	Fatty Acid
FAD	Flavin adenine dinucleotide
FMN	Flavin mononucleotide
FOXO	The Forkhead-O-box (FOXO) family of transcription factors
GRP	Genetic reference population
GXE	Gene-by-environment interaction
HFD	High fat diet
HPLC	High-performance liquid chromatography
IDO	Indoleamine 2,3-dioxygenase
LDL	Low density lipoprotein
LRS	Likelihood ratio statistic
MS	Mass spectrometry
NA	Nicotinic acid
NAAD	Nicotinic acid adenine dinucleotide
NAD	Nicotinamide adenine dinucleotide
NADP	Nicotinamide adenine dinucleotide phosphate
NAFLD	Nonalcoholic fatty liver disease
NAM	Nicotinamide
NAMN	Nicotinic acid mononucleotide
NAMPT	Nicotinamide phosporibosyltransferase
NAPRT	Nicotinic acid phosphoribosyltransferase
NASH	Nonalcoholic steatosis
NMNAT	Nicotinamide mononucleotide adenylyltransferase
NR	Nicotinamide riboside
PARPs	Poly(ADP-ribose) polymerases
PGC-1α	Peroxisome proliferator-activated-receptor- -coactivator 1α
PRPP	5-phospho-α-D-ribose 1-diphosphate
QTG	Quantitative trait gene
QTL	Quantitative trait loci
SIRT	Silent information regulators
TCA	Tricarboxylic acid
TDO	Tryptophan 2,3-dioxygenase (TDO).
Trp	Tryptophan
UPLC	Ultra-Performance Liquid Chromatography
WAT	White adipose tissue

WHO World Health Organization

Abstract

The prevalence of overweight and obesity increases worldwide due to a progressively sedentary lifestyle and the intake of high-fat energy dense diets. Moreover, both syndromes are linked to the development of metabolic disorders such as diabetes type II. The NAD^+-consuming family of sirtuins is able to modulate metabolic function. Hence, altering NAD^+ metabolism to modulate sirtuins could be an interesting way to enhance mitochondrial function and as a consequence, to burn more energy. The goal of this thesis is to map the quantitative trait loci (QTL) and underlying quantitative trait genes (QTGs) responsible for the regulation of the NAD^+ levels in the liver.

The qualitative and quantitative method to measure NAD^+ is validated *in vitro* and *in vivo*. NAD^+ is extracted from the liver of the BXD mouse genetic reference population (GRP) on chow (CD) and high fat diet (HFD) using an acidic and alkaline extraction method. The levels of NAD^+ are then analyzed on a LC-MS/MS. QTL mapping is performed with GeneNetwork and R.

Since no correlation between NAD^+ levels in both diets is observed, it is concluded there is no strong genetic effect on the NAD^+ regulation. Thus, suggestive QTLs are located on 2 loci in BXD on CD and on 3 loci in BXD on HFD. 229 underlying QTGs are eligible for NAD^+ regulation. Future network and correlation analysis would allow to identify new networks modulating NAD^+ levels. Eventually this opens perspectives to develop drugs against obesity and metabolic dysfunction that target gene(s) under the QTL.

Abstract in het Nederlands

Als gevolg van een toenemende sedentaire levensstijl en de inname van vet- en energierijke voeding lijden wereldwijd steeds meer mensen aan overgewicht en, in een gevorderd stadium, aan obesitas. Deze ziektes verhogen bovendien de kans op de ontwikkeling van diabetes type II en cardiovasculaire aandoeningen. Sirtuins reguleren de metabolische activiteit en verbruiken hierbij NAD^+. Onderzoek toont aan dat een verhoging in NAD^+ levels de activiteit van sirtuins stimuleert, waardoor de verbranding van suikers en vetten versnelt. Deze thesis tracht de locus (QTL) en genen (QTG) in kaart te brengen die verantwoordelijk zijn voor de regulatie van de NAD^+ levels.

Een NAD^+ methode werd gevalideerd *in vitro* en in het C57BL/6J muizen ras (*in vivo*). Vervolgens werd NAD^+ geëxtraheerd uit de lever van de BXD muizenpopulatie op een chow en vetrijk dieet, met behulp van een zuurbase extractie. Via LC-MS/MS werden de NAD^+ levels gekwantificeerd. QTL analyse werd uitgevoerd met GeneNetwork en R.

De NAD^+ levels in BXD op beide diëten correleren niet. Hieruit wordt afgeleid dat er geen sterke genetische invloed is op de NAD^+ regulatie. BXD op een chow diet bezitten 2 mogelijke QTLs in de chromosomen terwijl in BXD op een vetrijk dieet 3 loci geïdentificeerd worden. Hieronder bevinden zich 229 QTGs die in aanmerking komen voor NAD^+ regulatie. Toekomstige netwerk en correlatie analyse laat toe om nieuwe NAD^+ regulerende pathways te onthullen. Dit opent perspectieven om een medicijn te ontwikkelen tegen obesitas dat zich op deze genen richt.

1 Introduction

Diet, nutrition and physical activity are necessary for the maintenance of good health throughout the entire course of life. Since the second half of the 20th century, major changes have occurred in lifestyle of people in industrial regions and more recently in developing countries (World Health Organization (WHO), 2016a). Traditional, plant-based diets have been replaced by high-fat, high energy diets and lifestyle has progressively become more sedentary (Manco, M. et al., 2004). The direct consequence of these changes is an increase in the prevalence of overweight and obesity that are tightly associated to the development of metabolic disorders which includes chronic cardio-metabolic diseases, such as type II diabetes, cardiovascular diseases, atherosclerosis or nonalcoholic fatty liver disease (NAFLD) (Gariani, K. et al., 2016), (Verdin, E., 2015), (Houtkooper, R.H. et al., 2012). Mitochondrial dysfunction is one of the features of these metabolic and age-related diseases.

The liver is a central organ for metabolism, including roles in lipogenesis, gluconeogenesis and cholesterol metabolism (Bechmann, L.P. et al., 2012), (Gariani, K. et al., 2016). Also it plays a major role in oxidative metabolism. Energy within hepatocytes is provided by the mitochondria. In most metabolic pathways nicotinamide adenine dinucleotide (NAD^+) acts as a coenzyme during redox reactions and as a cosubstrate to other enzymes (Cantó, C. et al., 2015), (Verdin, E., 2015). The amino acid tryptophan, nicotinic acid (NA), nicotinamide (NAM) and nicotinamide riboside (NR) have been recognized as precursors in different pathways that form NAD^+ (Cantó, C. et al., 2015). In contrary to glycolysis where NAD^+ is converted into NADH, sirtuins catalyze the removal of acetyl groups from lysines on histones and proteins, while using NAD^+ as a substrate and releasing it in the form of NAM. Sirtuins, located in mitochondria and nuclei of cells, have come into the spotlight because of their ability to modulate metabolic function as they enhance mitochondrial metabolism by deacetylating transcription factors, cofactors and histones **(Figure 1).** Further evidence includes the prevention of metabolic complications such as obesity when overexpressed in mice (Cantó, C. et al., 2015).

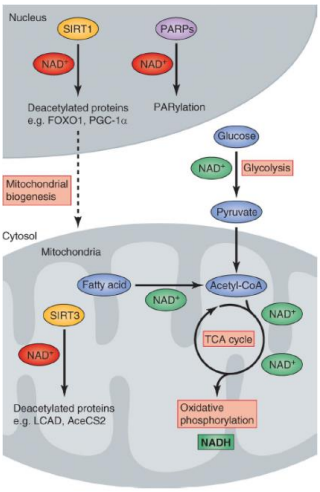

Figure 1: Both poly (ADP-ribose)-polymerases (PARP) and sirtuins (SIRT) are NAD+ degrading enzymes located in the mitochondria and nuclei of cells, releasing NAM (Houtkooper, R.H. & Auwerx, J., 2012).

The NAD^+/ sirtuin pathway adapts metabolism in response to environmental changes. NAD^+ levels rise during caloric restriction such as fasting and exercise (Houtkooper, R.H. & Auwerx, J., 2012). In contrary, a high-fat diet results in energy overload and NAD^+ levels are lower (Cantó, C. et al., 2015).

Altering NAD^+ metabolism to modulate sirtuins could be an interesting way to enhance mitochondrial function and as a consequence burn more energy (Houtkooper, R.H. & Auwerx, J., 2012). Research has shown that in mice, fed on a high-fat high sucrose diet supplemented with the NAD^+ booster NR, a sirtuin-dependent induction of mitochondrial proteins is observed. This triggers an increase in mitochondrial activity and function (Gariani, K. et al., 2016).

Complex traits such as obesity are the result of the interaction between genetic and environmental factors. One of the best mammalian models to study these gene-by-environment interaction (GXE) is the BXD mouse genetic reference population (GRP). The BXD family descends from crosses between a C57BL/6J mother (B) and a DBA/2J father (D) and is composed of ~160 lines. This mouse family models some aspects of human genetic diversity and is segregating for ~5 million common sequence variants, similar to many human populations (e.g., Icelandic) (Andreux, P.A. et al., 2012).

The systematic analysis of NAD^+ levels in the livers of all the BXD strains via LC-MS/MS would allow to identify genetic loci that control the NAD^+ levels using quantitative trait loci (QTL) mapping methods. Knowing the genes located under these QTL would open perspectives to use them as targets to screen and develop drugs against. Such drugs could be useful in diseases linked to altered NAD metabolism, such as obesity and its associated disorders.

The goal of this project is to map the QTL and Quantitative trait genes (QTGs) responsible for the NAD^+ levels. Therefore a qualitative and quantitative method to extract and measure NAD^+ levels from the livers of 50 BXD strains, fed on normal chow diet (CD) or with high-fat diet (HFD) for 20 weeks, has been developed. The high-fat diet resembled the Western diet consisting of high-fat and high-sucrose levels. We first established an LC-MS/MS protocol to measure NAD^+ levels. *In vitro* validation of our technique to measure NAD^+ levels took place, using samples of the mouse hepatocyte AML-12 cell line. We then measured NAD^+ levels in livers of 54 strains of the BXD Genetic reference population by LC-MS/MS. With this data on NAD^+ levels in the BXDs, QTL and QTGs are mapped. Genes under the QTLs have been further analyzed for their role in NAD^+ metabolism. Network and correlation analysis from the NAD^+ levels was performed with the phenotypic, microarray, proteomics, metabolomics and lipidomics data, which are already available from these mice on GeneNetwork (http://www.genenetwork.org/). Such kind of analysis allows to validate the already known correlations and networks and also identify new networks which could modulate NAD^+ levels.

2 Literature study

2.1 Obesity

During the last 40 years the prevalence of obesity has already doubled worldwide. The World Health Organization (WHO) indicates that 39 % or 1,9 billion adults are overweight and more than 13 % or 600 million people suffer from obesity (World Health Organization, 2016b). The extent to which someone is overweight is expressed in the body weight index (BMI). Anybody with a BMI higher than 25 kg/ m^2 is considered overweight. A BMI above 30 is considered obese. Over the years the problem of obesity has become increasingly important in developing countries because of growing economies, an increase of daily income and sedentary lifestyle. Worldwide more people die suffering from the consequences of overweight and obesity than from underweight (Balentine, J. & Conrad, M., 2016)((World Health Organization, 2016b), (Verduin, P. et al., 2005).

Obesity-related diseases are type 2 diabetes, cardiovascular diseases (Verdin, E., 2015) and nonalcoholic fatty liver disease (NAFLD) (Gariani, K. et al., 2016). A study reports (Harvard T.H. Chan, 2016) about the increasing risk of developing diabetes among women who had a BMI of 35 or higher. This risk has been proven to be 93 times higher in comparison with women who had a BMI lower than 22. Adipose tissue has proven to interact with the inflammatory system. In regular state this system provides a rapid response to a site of injury or infection. After solving the problem, the inflammatory response is neutralized. In obesity, the extensive intake of nutrients causes an inappropriate induction of inflammation, inducing various health problems such as making the body less responsive to insulin. This results in higher blood sugar levels and eventually the prevalence of diabetes (Harvard T.H. Chan, 2016), (Gregor, M.F. & Hotamisligil, G.S., 2011).

Moreover other obesity-associated health risks include an elevated blood pressure and an increased amount of low density lipoprotein (LDL) and triglycerides in the blood. This could lead to atherosclerosis, a stroke and eventually death (Harvard T.H. Chan, 2016).

2.2 Metabolism

The metabolism consists of central pathways designed to process carbohydrates, fatty acids and amino acids. A pathway is considered catabolic or anabolic. In catabolic pathways nutrients are degraded to elementary molecules like CO_2, NH_3 or H_2O. The chemical energy released during this breakdown is captured in the form of ATP. In anabolic pathways, ATP is consumed to form complex products such as proteins or lipids. The biosynthesis pathway and degradative pathway usually differ from each other and are regulated by various regulatory intra- and extracellular signals. (Richard A Harvey (Ph D) et al., 2011).

During digestion, nutrients such as carbohydrates, fatty acids and proteins are hydrolyzed to their respective building blocks. In the gut they are absorbed and transported to the liver via the hepatic portal vein. The liver processes the nutrients and distributes them to the rest of the body. After consuming a carbohydrate-rich meal, the hepatic metabolism

enhances the glycolysis and the biosynthesis and storage of glycogen. Thereby it is coordinating with other pathways such as gluconeogenesis. Moreover during a well-fed state, the liver will synthesize fatty acids and triglycerides. The liver is also involved in the metabolism, processing and release of lipoproteins. Next it regulates the amino acid degradation in case of excessive intake and protein synthesis. In the cell cytoplasm glucose is broken down to pyruvate, Acetyl CoA or other intermediates while generating ATP. Acetyl CoA is also connected to the metabolism of amino acids and fatty acids. Acetyl CoA, produced at the end of the glycolysis can be further metabolized in the Krebs cycle or tricarboxylic acid (TCA) cycle to CO_2 and H_2O. The cycle is located in the mitochondria of cells and counts when coupled with oxidative phosphorylation (see below) for almost 2/3 of total ATP production (Richard A Harvey (Ph D) et al., 2011).

2.2.1 Mitochondria

2.2.1.1 *Structure*

The mitochondrion is built of two membrane layers of phospholipids. The outer membrane is selective permeable to ions and small molecules while the inner membrane contains special transport systems to transport ions. The surface is increased by many cristae (Richard A Harvey (Ph D) et al., 2011).

2.2.1.2 *Electron transport chain (ETC) and oxidative phosphorylation*

During the oxidation of energy-rich nutrients, their electrons are transferred to nicotinamide adenine dinucleotide (NAD^+) or flavin adenine dinucleotide (FAD). Cytoplasmic NADH from glycolysis is transported via the glycerol-3-phospate shuttle or the malate-aspartate shuttle into the mitochondria. In complex I, located in the inner mitochondrial matrix, NADH dehydrogenase catalyzes the reaction of NADH to NAD^+ while the hydrogen atoms are accepted by flavin mononucleotide (FMN). $FMNH_2$ transfers both electrons to ubiquinone. Next they are relayed along cytochrome b, c and a + a_3. The ETC is coupled to the realization of a proton gradient and pH gradient. Protons are pumped from the mitochondrial matrix to the intermembrane space. The generated energy will drive ATP synthesis (Richard A Harvey (Ph D) et al., 2011), (Cantó, C. et al., 2015). The mitochondrial complexes are placed on the inner membrane. The matrix contains TCA enzymes, fatty acid oxidation enzymes, mitochondrial DNA (mtDNA) and RNA and mitochondrial ribosomes (Richard A Harvey (Ph D) et al., 2011).

2.3 Nicotinamide adenine dinucleotide (NAD^+)

As described above, NAD^+ **(Figure 2)** is a metabolite present in different cellular compartments, transferring hydrogen in biochemical reactions catalyzed by numerous oxidoreductase enzymes (Cantó, C. et al., 2015). NAD^+ is mainly bound to intracellular proteins but it is also found in free state (Houtkooper, R.H. et al., 2010). NAD^+ modulates the activity of different metabolic pathways (Mouchiroud, L. et al., 2013). In glycolysis NAD^+ is reduced to NADH during the oxidation of glyceraldehyde-3-phosphate to 1, 3-diphosphoglycerate while in the mitochondrial TCA cycle multiple NAD^+ are reduced. NADH can be oxidized via the lactate dehydrogenase reaction, as in erythrocytes (Houtkooper, R.H. et al., 2010), or via the mitochondrial electron transport chain (ETC) generating ATP, the primary biological form of energy in organisms. Depending on the

tissue and cell type, the intracellular NAD^+ level varies between 0,2 and 0,5 mM(Srivastava, S., 2016; Cantó, C. et al., 2015). Between the interconversion of NAD^+ and NADH there is no net consumption of NAD^+ (Cantó, C. et al., 2015).

Beside its role as a coenzyme in energy metabolism, NAD^+ has been proven to act as cosubstrate to enzymes involved in cell regulation: ADP-ribose transferases such as Sirtuins, poly (ADP-ribose) polymerases (PARPs) and cyclic ADP (cAPD) ribose synthetases. These NAD^+ consuming enzymes regulate metabolism by modifying proteins donating the ADP-ribose group from NAD^+. Physiological changes in NAD^+ levels adjust the activity of these enzymes. NAD^+ formation is required in order to avoid depletion of the cellular NAD^+ levels (Houtkooper, R.H. et al., 2010). Several biosynthetic pathways are documented.

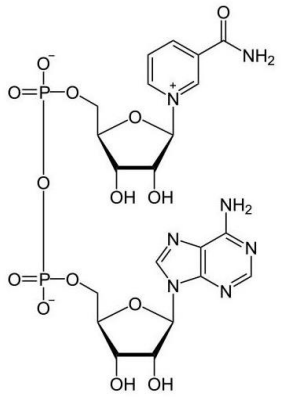

Figure 2: The structure of NAD^+ (True Life Research, 2016)

2.3.1 NAD^+ biosynthesis

Tryptophan (Trp), nicotinic acid (NA), nicotinamide and nicotinamide riboside have been described as root compounds in the synthesis of NAD^+ (Cantó, C. et al., 2015). Trp is an essential amino acid, which is common in nuts, seeds, soya beans etc.(Whitbread, D., 2016). The entire biosynthesis pathway is described in **Figure 3.** It starts with the conversion of tryptophan to N-formulkynurenine catalyzed by indoleamine 2, 3-dioxygenase (IDO) or tryptophan 2, 3-dioxygenase (TDO). Subsequently during four steps, N-formylkynurenine is transformed to the unstable α −amino-β −carboxymuconate-ε −semialdehyde, which subsequently undergoes a spontaneous cyclization to quinolinic acid (Houtkooper, R.H. et al., 2010). Finally quinolinic acid is condensed with 5-phospho-α-D-ribose 1-diphosphate (PRPP), forming nicotinic acid mononucleotide (NAMN). Next NAMN is converted to nicotinic acid adenine dinucleotide (NAAD). Finally NAD^+ is formed during the amidation of NAAD by the NAD synthase enzyme in the Preiss-Handler (Houtkooper, R.H. et al., 2010), (Mouchiroud, L. et al., 2013). Nevertheless the bulk amount of NAD^+ is synthesized in the salvage pathways starting from other NAD^+ precursors. In humans, 1 mg of niacin consisting of NA, nicotinamide (NAM) and nicotinamide riboside (NR) results in an equal amount of NAD^+ as 34 to 84 mg of Trp. The lower efficiency of Trp in NAD^+ biosynthesis is due to its use in protein translation. (Cantó, C. et al., 2015).

Nicotinic acid is considered the starting point of the Preiss-Handler pathway described earlier. NA phosphoribosyl transferase (NAPRT) catalyzes the conversion of NA to NAMN using PRPP. The next steps in this pathway leading to NAD^+ are similar as described earlier (Houtkooper, R.H. et al., 2010).

The synthesis from nicotinamide (NAM) or nicotinamide riboside (NR) happens during only two steps each. Phosphorylation of NR by one of NR kinases results in the formation of Nicotinamide mononucleotide (NMN) (Ross, Zibadi, & Victor, 2010). NAM is converted into NMN by nicotinamide phosphoribosyl transferase (NAMPT) using PRPP as a substrate. After that one of the NAM mononucleotide adenylyl transferase (NMNAT) enzymes catalyzes the conversion of NMN to NAD^+(Houtkooper, R.H. et al., 2010), (Cantó, C. et al., 2015).

The substrate preference for NAD^+ formation depends of the presence of their respective enzymes in the different tissues. It was shown that in liver the NAPRT enzyme is most active. Thus NA can act as the primary precursor (Houtkooper, R.H. et al., 2010), (Cantó, C. et al., 2015). However, blood levels of NA are generally very low so that mammalian tissues absorb little. Similar to NA it was proven that the level of NAM in the blood is not sufficient to enhance NAD^+ biosynthesis *in vitro* (Cantó, C. et al., 2015).

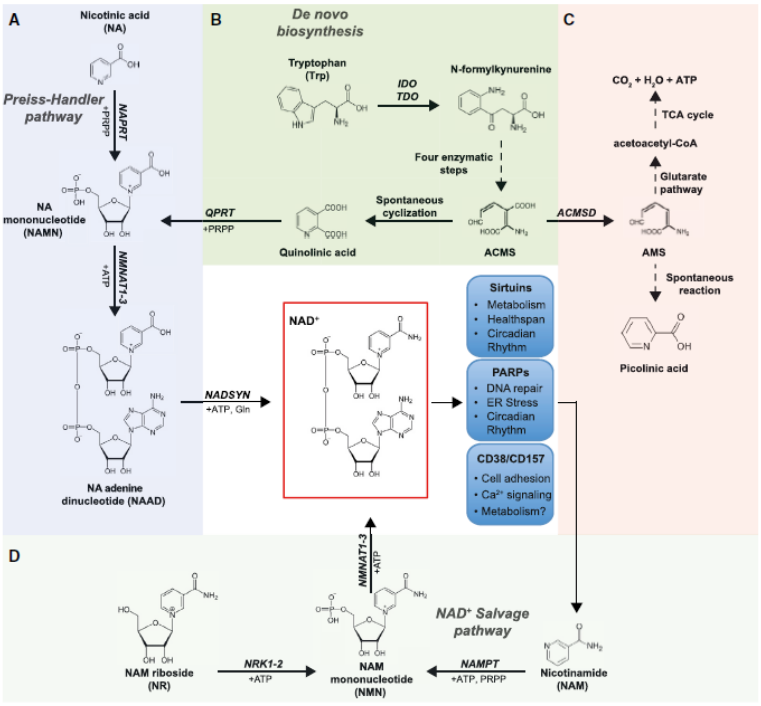

Figure 3: The NAD^+ precursor Trp is converted into NAD^+ in the de novo biosynthesis pathway. This pathway connects to the Preiss-Handler pathway, which starts from NA. NAM and NR are both converted to NMN. NAD^+ is formed from NMN by the NMANTs (Cantó, C. et al., 2015).

2.3.2 NAD^+ consuming enzymes

In general sirtuins, Poly (ADP-ribose) polymerases (PARPs) and Cyclic ADP (cADP) ribose synthetases use NAD^+ as a substrate. As will be described in the following chapters, these

enzymes are responsible for multiple processes such as protection against traumatic stress or resistance to cell apotheosis. Altering the NAD^+ metabolism and therefore the available intracellular NAD^+ pool could modulate the activity of these enzymes and hence, these processes (Yang, B. & Kirchmaier, A.L., 2006).

2.3.2.1 *Sirtuins*

Sirtuins or Silent Information Regulators (SIRT) proteins are a NAD^+ -consuming family of enzymes removing acetyl groups from lysine residues on histones and proteins. During the reaction NAD^+ is cleaved into nicotinamide and O-acetyl adenosine diphosphate ribose. Also the deacylated substrate is released **(Figure 4).** Seven sirtuins have been described in mammals. One characteristic of Sirtuins is their high K_M for NAD^+. This indicates that NAD^+ is a rate-limiting substrate for the reaction (Cantó, C. et al., 2012). The difference between each sirtuin lies in their respective location, function and target (Cantó, C. & Auwerx, J., 2012).

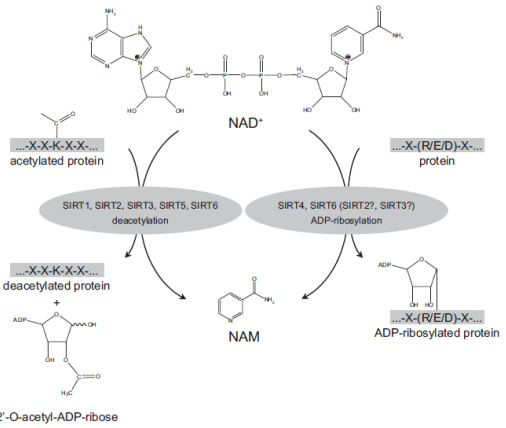

Figure 4: SIRT 1, 2, 3, 5 and 6 cleave NAD^+ into NAM, O-acetyl ADP ribose and a deacetylated substrate. SIRT4 and 6 cleave NAD^+ into an ADP-ribosylated protein and NAM (Houtkooper, R.H. et al., 2010).

Over the years SIRT1 has become the best-characterized orthologue of the sirtuin family. Its location differs between the nuclear and cytosolic cell compartment depending on the tissue or cell type (Cantó, C. et al., 2012). Like SIRT2 and 3, SIRT1 has a high enzymatic deacetylase activity (Cantó, C. & Auwerx, J., 2012). Through deacetylation SIRT1 inhibits or activates transcriptional regulators although its main activity involves mitochondrial biogenesis and stress response through the deacetylation of the peroxisome proliferator-activated-receptor- γ-coactivator 1α （PGC-1α), a transcriptional regulator for glucose production (Mouchiroud, L. et al., 2013). Furthermore SIRT 1 is able to regulate cholesterol metabolism such as lipid and cholesterol homeostasis by deacetylating the nuclear receptor LXR (Imai, S.I., 2009). Other significant SIRT1 targets in stress response are p53, HIF-1α, and NF-κB (Mouchiroud, L. et al., 2013). Studies show that genetically engineered mammals with enhanced SIRT1 activity are better secured against the development of certain types of cancer (Cantó, C. & Auwerx, J., 2012).

A specific example of a transcription regulator of which SIRT1 determines the activity is the Forkhead-O-box (FOXO) family of transcription factors. FOXOs regulate lipid metabolism, apoptosis and stress resistance (Cantó, C. & Auwerx, J., 2012). Deacetylation of FOXO3 by SIRT1 inhibits the apoptosis related gene expression while enhancing

autophagy. Also it was shown that oxidative stress, energy stress and fasting prompt SIRT1 activity. This evidence indicates the link of SIRT1 deacetylation and energy stress and metabolism (Cantó, C. & Auwerx, J., 2012).

SIRT2 is localized in the cytoplasm while SIRT6 and 7 are nuclear proteins. SIRT2 is known to control gluconeogenesis and interfere in the TNFα-mediated necrosis pathway. (Houtkooper, R.H. et al., 2010), (Cantó, C. et al., 2015) (Mouchiroud, L. et al., 2013). SIRT 3-5 are found in the mitochondria and fulfill deacetylation of proteins in the pathways of mitochondrial metabolism such as oxidative phosphorylation, fatty acid oxidation, ketogenesis etc. (Mouchiroud, L. et al., 2013). SIRT6 is able to catalyze the removal of succinyl, malonyl and glutaryl groups. Finally SIRT7 is an NAD^+ -dependent deacetylase with only few known substrates (Cantó, C. et al., 2015).

2.3.2.2 *Poly (ADP-ribose) polymerases (PARPs)*

ADP-ribosylation activities were first described (CHAMBON, P. et al., 1963) in 1963 by Chambon. He registered the transfer of the ADP-ribose group of NAD^+ to an amino acid acceptor while studying the stimulation of poly (ADP-ribose) by adding NAD^+ to liver nuclear extracts. PARPs catalyze the transfer of ADP-ribose groups of NAD^+ to protein targets involved in the maintenance of chromatin structure, DNA metabolism, inflammation and cell death (Houtkooper, R.H. et al., 2010) **(Figure 5).** Before executing its main reaction, PARP must be activated. The activation via DNA strand break allows them to fulfill its role in repair mechanisms. A second option is via interaction with phosphorylated extra signal-regulated kinases. A third described option is the activation by HSP70 during heat shock stress (Cantó, C. et al., 2015).

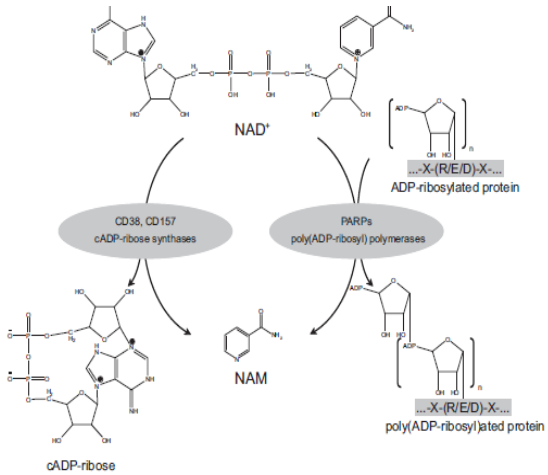

Figure 5: PARPs catalyze the transfer of ADP-ribose moieties of NAD^+ to protein targets involved in the maintenance of chromatin structure, DNA metabolism, inflammation and cell death and C38 cleaves NAD^+ into a cADP-ribose and NAM (Houtkooper, R.H. et al., 2010).

2.3.2.3 *Cyclic ADP (cADP) ribose synthetases*

Cyclic ADP (cADP) ribose synthetases such as CD38 or CD157 are enzymes that use NAD^+ as a substrate to produce cADP, a secondary messenger involved in Ca^{2+} signaling (Cantó,

C. et al., 2015). CD38 and 157 are antigens that are typically found in lymphoid tissues. However research showed it presence also in brain, liver and muscle. The NAD^+ depleting role of C38 was proven by knocking out the CD38 gene in mice, which led to a rise in NAD^+ levels. In turn energy expenditure was elevated in these mice due to an increased SIRT1 activity protecting them from diet-induced obesity (Pfluger, P.T. et al., 2008), liver steatosis and glucose intolerance. In contrary, CD38 overexpression resulted in a decrease of NAD^+ levels (Cantó, C. et al., 2015), (Houtkooper, R.H. et al., 2010). Boosting the metabolism by elevating NAD^+ levels

A recent study shows the effect of NR on intracellular NAD^+ levels (Cantó, C. et al., 2012). Increasing availability of NAD^+ through NR supplementation leads to SIRT1 and SIRT3 activation. This stimulates the metabolism and protects against high-fat induced obesity. This hypothesis was tested by exposing mice and human cell lines to a treatment of the NAD^+ precursor NR. Here, an cellular and mitochondrial increase of NAD^+ level was detected. This latter was not the case when PARP was inhibited aiming to increase the amount of NAD^+. Moreover, NR treatment didn't affect the PARP activity indicating that the increasing NAD^+ level is due to enhanced biosynthesis and not by a disturbed NAD^+ consumption. In contrary SIRT1 and 3 activity were elevated resulting in a higher expression of target genes (Cantó, C. et al., 2012). Other research confirms this research by putting PARP1 and PARP2 knockout mice on a HFD. They were protected from high-fat diet induced obesity due to elevated NAD^+ levels and increased SIRT1 activity in brown adipose tissue (BAT) and muscle (Mouchiroud, L. et al., 2013).

The effect of NR treatment, on mice fed on a HFD or CD, on body weight gain is due to a reduced fat mass. This effect could be explained by an elevated 0_2 consumption resulting in enhanced energy expenditure. (Cantó, C. et al., 2012).

Both white adipose tissue (WAT) and brown adipose tissue (BAT) have been recognized for their role in fat storage. BAT contains many mitochondria driving ATP synthesis.. The produced heat is distributed to the whole body. Because of the tight concentration of mitochondria and thermogenesis, BAT is an important target for metabolic diseases such as obesity (Harms, M. & Seale, P., 2013). Upon NR supplementation in a CD or HFD diet, mice were able to to resist a cold exposure by maintaining body temperature because of more abundant cristae in the structure of BAT. Overall, it was proven that the mitochondrial function was improved (Cantó, C. et al., 2012).

Upon feeding mice with a chronic NR supplemented diet, NAD^+ increases or remained the same depending of the tissue. The NAD^+ levels are increased in liver and muscle of mice on CD and HFD but not in brain and WAT tissue. Only in BAT tissue of mice on HFD diet, NAD^+ levels rise. This can be due to a different tissue-dependent expression of NRK's. These enzymes catalyzed the conversion of NR to NMN in the NAD^+ biosynthesis. A rise in mitochondrial protein amount can be explained by an enhanced biogenesis of mitochondria. This result links the higher amount mitochondria in the NAD^+ risen tissues to the higher energy expenditure in NR supplemented HFD fed mice (Cantó, C. et al., 2012).

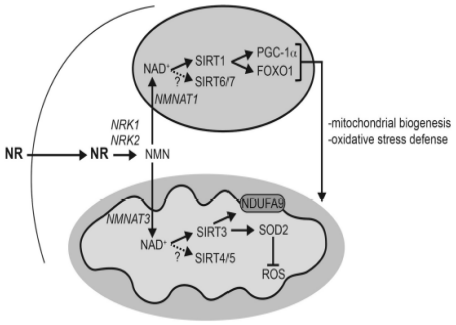

Figure 6: Elevating the intracellular NAD+ levels via NR treatment enhances SIRT1 activity. An increase of SIRT1 activity results in the rise of transcriptional activation of FOXO1 and PGC-1α by their deacetylation. The biogenesis of mitochondria will enhance. In general, this effect protects from high-fat diet induced obesity (Cantó, C. et al., 2012).

2.4 Modulation of NAD+ levels by physiological processes

Physiological stimuli drive metabolic adaptions. During caloric restriction NAD+ increases because fewer nutrients are available for oxidation and subsequently NADH production. The low availability of glucose must be compensated by mitochondrial fatty acid oxidation to maintain blood glucose levels providing other tissues of energy. In response to energy deficiency, AMP-activated protein kinase (AMPK) a sensor for the intracellular AMP/ATP ratio, will regulate mitochondrial biogenesis. Through AMPK actions in lipid oxidation, intracellular NAD+ levels rise, thereby AMPK enhances SIRT1 activity. This results in the deacetylation of SIRT1 targets: PGC1-α or the FOXO family(Cantó, C. et al., 2010). These regulate in its turn genes involved in mitochondrial and lipid metabolism (Cantó, C. et al., 2009).

Excessive caloric intake such a HFD leads to reduced NAD+ levels due to elevating energy availability and NADH production. Fatty acids are degraded in mitochondria through β-oxidation. Excess lipids are stored in adipose tissue as triglycerides. HFD induces a decrease of lipid metabolism intermediates and NAD+/NADH ratio. This indicates that the metabolism is disturbed (Kim, H.J. et al., 2011).

2.5 Pharmacological control of NAD+ levels

2.5.1 NAD+ boosters

NA, NMN, NR are NAD+ precursors and boost NAD+ biosynthesis. PARP and C38 inhibitors block the consumption of NAD+. It was proven that a decrease in the level of NAD+ by blocking PARP, results in an increase of SIRT1 activity. PARP knockout mice are also protected against high-fat diet induced obesity as a result of an improved mitochondrial function (Mouchiroud, L. et al., 2013). A similar phenotype was reported in CD38 knockout mice (Camacho-Pereira, J. et al., 2016), (Barbosa, M.T.P. et al., 2007).

The effect of NAD+ precursors that act as NAD+ boosters, has already been recognized such as by their effectiveness in case of the disease Pellegra, which is characterized by diarrhea, dementia and eventually death. This disease is caused by an insufficient intake of dietary NAD+ precursors. Providing NA or NAM, present as vitamin B3 in our diet, helps to solve

this deficiency (Cantó, C. et al., 2015). Blood lipid and cholesterol levels also benefit from niacin (NA) intake. NR is found in milk. The advantageous effects of NR are described in 0.

2.5.2 Resveratrol

Polyphenol 3, 5, 4'-trihydroxystillbene or Resveratrol was isolated from the roots of the plant white hellebore and Japanese knotweed. It is also present in fruits such as grapes, blueberries and peanuts. Identification also occurred in red wine where it has been recognized as the molecule that is potentially responsible for the cardio protective effects linked with red wine consumption. Mice on HFD supplemented with resveratrol benefit from an improved glucose metabolism and less damage to pancreas and heart. These observations are associated with an improved AMPK and PGC1-α activity influencing mitochondrial biogenesis and energy expenditure **(Figure 7).** This results in an extended lifespan. Also resveratrol treatment has shown be to effective in the prevention and the delay of cardiovascular diseases and cancer (Mouchiroud, L. et al., 2013).

2.5.3 STACs

STACs are synthetic SIRT activating compounds such as SRT1720. HFD induced obese mice benefit from a decrease of weight gain and a longer life expectancy due to increasing SIRT1 activity when treated with STACs (Mouchiroud, L. et al., 2013)

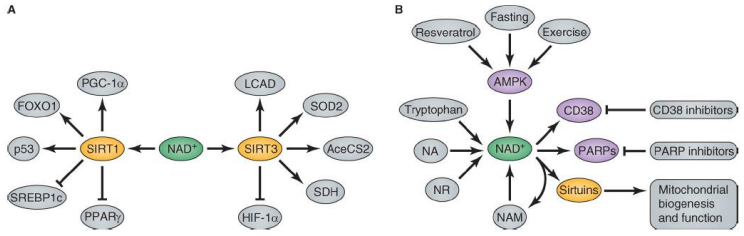

Figure 7: Modulating the NAD+ metabolism via pharmacological boosters, physiological stimuli and NAD+ precursors influence the NAD+ levels. This alteration affects the activity of NAD+ consuming enzymes.(Houtkooper, R.H. & Auwerx, J., 2012)

2.6 Metabolomics

2.6.1 Ultra-Performance Liquid Chromatography – Mass Spectrometry

The Thermo Scientific™ TSQ Quantum™Access MAX LC-MS **(Figure 8)** is used to quantify the amount of NAD+. It provides characteristics as speed, sensitivity, separation efficiency and chromatographic resolution to our analysis(Suman, S. et al., 2014).

Chromatography is a technique that has the ability to separate a mixture into individual components based on its physical and chemical interaction with the stationary phase in a column. As the separated compounds leave the column, they flow into a detector. Each peak corresponds to a component in the mixture and appears at a specific retention time. The peak area is an indication for the concentration (Suman, S. et al., 2014), The LC is coupled to a MS/MS instrument. The most important characteristic of MS is the ability to identify a compound present in an extremely small concentration (Patil, V. et al., 2011).

Figure 8: The Thermo Scientific™ TSQ Quantum™ Access MAX LC-MS (ThermoFisher, 2015)

A triple-quadropole mass spectrometer sorts analytes according to mass-to-charge ratios. First the sample is introduced in the ion source **(Figure 9)** and broken and ionized into fragments. The ions are accelerated by an eletric pulse. Next in row are three quadroples from which the first and thirth act as mass filter based on the application of a certain ac en dc. The second quadrole cleaves ions in fragments through interaction with a collision gas (Labcompare, 2009). Every ion of the selected mass that passes by the mass filter is detected with an electron multiplier. These fragments are displayed and recorded into a spectrum (Kinesis, 2016).

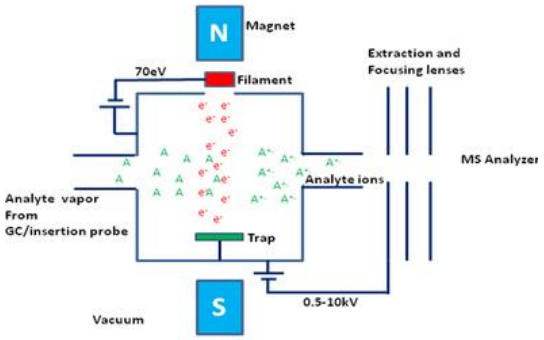

Figure 9: Molecules separated on the column enter the ion source via the needle. The sample is broken and ionized into fragments and these are subsequently accelerated. They are led into the first quadrupole (University of Pittsburgh, 2016)

2.7 Bio-informatics

2.7.1 GeneNetwork

GeneNetwork is a webportal that contains both bio-informatics tools combined with large data sets from human, mice, rats, Drosophila and plant species uploaded by the wider scientific community. The datasets range from phenotypic data to transcriptome, proteome, metabolome and microbiome. Together with sequence data (SNPs), the omics data-sets are used to study complex networks of genes and molecules. It allows to determine the influence of gene variants and environmental factors on phenotypes (clinical and molecular) by identifying quantitative trait loci (QTL) that are informative about the phenotypes. Linking the data sets to genotypes results in the location of genetic modifiers that cause differences in gene expression and clinical phenotypes (GeneNetwork, 2016).

3 Experimental Procedures

3.1 NAD^+ extraction method

3.1.1 Protocol for cell extraction

The cells were scraped from the plate using 250 µL of $HClO_4$ 10% (Sigma) per well. The solution was collected and centrifuged at 15300 rpm (4 degree) for 5 min. The supernatant was isolated and 150 µl of 3M K_2CO_3 (Fisher Scientific) was added. The samples were vortexed, kept on ice for 10 min and subsequently centrifuged at 15300 rpm (4 degree) for 5 min. The same volume of supernatant of each sample was separated and stored at -80°C.

3.1.2 Protocol for tissue extraction

500 µl of $HClO_4$ 10% (Sigma) and 20 µl of 600 µM of 2-chloro adenosine (Sigma) were added to each frozen tissue sample (ratio; tissue 20 mg / $HClO_4$ 500ul). The tissues must not be defrosted before adding $HCLO_4$ to avoid degradation. The samples were extensively homogenized with the tissue-lyser (Qiagen) until homogenization of all the tissue (1-2 min). Thereafter the samples are kept on ice for 15 min and centrifuged at 15300 rpm for 5 min (4 degree). The supernatant was isolated and 150 µl of 3M K_2CO_3 (Fisher Scientific) was added. The samples were vortexed, kept on ice for 10 min and subsequently centrifuged at 15300 rpm for 5 min (4 degree). The supernatant of each sample was collected and stored at -80°C.

3.2 LC-MS/MS analysis

3.2.1 Materials

NAD^+ and 2-chloro-adenosine were purchased from Roche and Sigma, respectively. Ultrapure water was prepared using a Milli-Q water system. HPLC-grade methanol and acetonitrile were also obtained from Sigma. Ammonium acetate was purchased from Fluka. The pH is adjusted with ammonium hydroxide solution (>25% in H_2O, eluent additive for HPLC, Fluka).

3.2.2 Instrumentations

LC-MS/MS was performed using a TSQ Quantum™ Access MAX Triple Quadrupole Mass Spectrometer (ThermoFisher Scientific). All compounds were separated over a Kinetex 5µM EVO C18 100 Å LC column of 150 x 2,1 mm (Phenomenex). The mobile phase consists of 20 mM acetate in ultrapure H_20 at pH 9,4 (A) and 5 mM ammonium acetate in methanol at pH 8,5 (B). NAD^+ was separated using a linear gradient that started at 100 % A and ended at 11 minutes. Next the mobile phase was held at 100 % B for 4 minutes. At last the mobile phase returned to 100 % A at 17 minutes and stayed this way until 25 minutes. The flow rate was 300 µl/ min at all time and the injection volume was 10 µl.

The capillary temperature was 270°C and the vaporizer temperature was set at 420°C. The aux gas pressure is kept at 10 bar while the sheath gas pressure was 35 bar. The spray voltage was set at 3500 V. The m/z range monitored between 664 (parent ion) and 135

(product ion) for NAD^+ and at 320,7 for 2-chloro-adenosine. A standard calibration curve was used to determine the unknown NAD^+ concentration in the samples. Xcalibur was used for data processing. The elution time of NAD^+ lied at 3.29 minutes.

3.2.3 Preparation of calibration standards

A NAD^+ stock solution was prepared in a mix of 4:1 $HClO_4$, 10 % and 3 M K_2CO_3. This solution was prepared in advance by slowly adding $HClO_4$ to K_2CO_3 and subsequently the mix was kept on ice for 10 minutes. Next it was centrifuged at 15'000 rpm for 5 minutes at 4°C. Finally the supernatant is taken. The calibration standard exists of final amounts of 20, 10, 5; 2,5; 1,25; 0,625 µM. The standard at 5 µM is aliquoted and stored at -80°C.

3.3 *In vitro validation*

3.3.1 Cell line

The mouse hepatocyte cell line AML12 cells (ATCC® CRL2254) was grown in a medium consisting of a 1:1 mixture of Dulbecco's modified Eagle's medium and Ham's F12 medium with 0,005 mg/mg insulin, 0,005 mg/ml transferrin, 5 ng/ml selenium and 40 ng/ml dexamethasone 90% and 10 % fetal bovine serum at 37°C.

3.3.2 Compound and treatment

Nicotinamide Riboside (NR) was purchased from Novalix (France). All the cell treatments with NR has been performed during 24 hours in a concentration range from 0,003mM to 10mM. The hydrogen peroxide (H202) was purchased from Emsure. The cells have been treated during 1 hour with 500uM H202.

3.3.3 EC_{50}

The EC_{50} calculation has been done using 8 different concentrations. To calculate the EC_{50}, the logarithm of the NR concentration has been plotted against the percentage of efficacy relative to the highest amount of NAD^+ at 10 mM NR. This latter is calculated according to **Equation 1.** Subsequently a nonlinear curve is fitted.

$$\% \text{ efficacy} = \frac{NAD\ (nM) - average\ NAD\ (nM) at\ 0\ mM\ NR}{average\ NAD\ (nM) at\ 10\ mM - average\ NAD\ (nM) at\ 0\ nm\ NR} * 100$$

Equation 1: % efficacy

3.4 *In vivo* validation

3.4.1 Mice treatment

To validate the sensitivity of the method C57BL/6J mice were treated for 4 weeks with 400mg of NR/kg of body weight in the diet and they were subsequently sacrificed. Liver samples were taken and extracted according to the protocol in 3.1.2. The samples were stored at -80°C.

3.4.2 Variation

Sixteen liver samples were collected and weighted from a C57BL/6J mouse. Next they were snap-frozen in liquid nitrogen and stored at -80°C. The tissues were extracted to the protocol in 3.1.2 and analyzed according to the method in 3.2. The NAD^+ levels were normalized to tissue weight ($\frac{\text{pmol of } NAD^+}{\text{mg tissue}}$), protein amount ($\frac{\text{pmol of } NAD^+}{\mu\text{g protein}}$) and internal standard 2-chloro-adenosine ($\frac{\text{pmol of } NAD^+}{\text{mg tissue}} * \frac{\text{IS final } (\mu M)}{\text{IS initial } (\mu M)}$). The precision of the method is expressed by the coefficient of variation (CV). This represents the relative standard deviation (RSD) calculated as the ratio of the standard deviation to the mean.

3.5 Protein concentration assay

The protein amount is used to normalize the NAD^+ data. Hence the protein concentration must be determined using a DC™ Protein Assay Reagents Package (Biorad) existing of protein Assay reagent A, protein Assay reagent B and protein Assay reagent S.

3.6 BXD

3.6.1 Animals

The BXD family **(Figure 10)** descends from crosses between a C57BL/6J mother and DBA/2J father. The resulting siblings are mated for at least 20 generations (Peirce, J.L. et al., 2004) until entire isogenic lines are obtained (Andreux, P.A. et al., 2012). Liver samples are obtained from the entire BXD genetic reference population (GRP), housed at the EPFL animal house (a total of 54 lines, with between 1 to 5 mice collected per line). The mice had been fed a CD or HFD for 28 weeks. Subsequently they have been sacrificed and all organs have been collected and stored at -80°C.

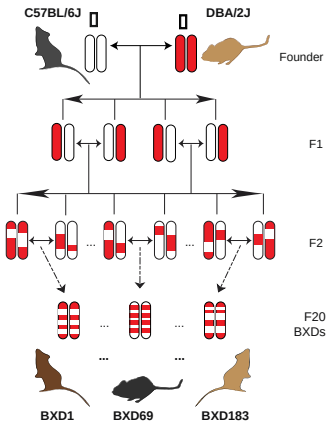

Figure 10: Breeding scheme of the BXD (Andreux, P.A. et al., 2012).

3.6.2 NAD^+ extraction and measurement

All BXD liver samples were distributed randomly in 17 batches of 28 samples. In each batch one control sample of 20 mg was included. These descend from the liver of a C57BL/6J, born on 27-02-2016, with code LIM IO8779 AAJ. This mouse had not been fasted before tissue extraction. The batches were extracted daily according to the protocol in 3.1.2. Next, each batch was divided in two LC-MS/MS sequences of 14 samples, one

control sample and a fresh standard of 5 μM NAD^+. The BXD extracts and the control were diluted ten times before being analyzed according to the protocol in 3.2. The standard was measured twice in each run.

3.6.3 Data analysis

The obtained raw NAD^+ values were corrected to the 5 μM standard in each run to cover the variation induced by the LC-MS/MS. Subsequently they were normalized to the protein amount. Thirdly, the NAD^+ values were multiplied with a batch factor. This corrects the variation induced by different batch extraction efficiency. Outliers are removed by boxplot analysis.

The data obtained by the MS measurement will first be analyzed for the normality in R. I will use Q-Q plot, Shapiro test and Hist function to test the normality of the data. If necessary the data will be log transformed before further analysis. The normalized data will be uploaded in Gene-network for QTL mapping. Parametric QTL mapping was performed since the data were normally distributed. Genes under the QTL were analyzed for cis-QTLs, and correlation with NAD^+.

4 Results

4.1 *In vitro* validation of the NAD^+ measurement

4.1.1 Positive validation

NR has been described as an intracellular NAD^+ booster in cell lines and tissues (Cantó, C. et al., 2012). It is proven that a treatment of NR at 1 mM induces a significant increase of NAD^+. To establish a reliable and reproducible protocol for the NAD^+ measurement in BXD samples, it is necessary to test if applying the measurement method to a cell line, treated with NR 1 mM, allows us to detect a rise of the level of NAD^+. To assess the significance we performed the unpaired t-test ($P< 0,05$). In case of significance it is represented with an asterisk (*).

The mouse hepatocyte cell line (AML-12) shows a significant increase of the NAD^+ level after 24 hours of treatment with NR (1mM). The results are displayed in **Figure 12.**

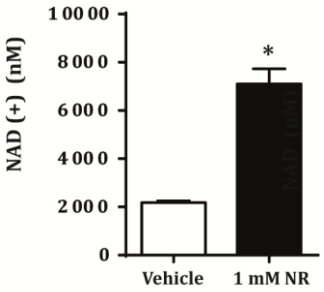

Figure 11: 24h treatment with a NAD^+ booster increases significantly intracellular NAD^+ levels in comparison to the non-treated vehicle.

We conclude that the applied extraction and measurement method allow the detection of the elevation of NAD+ under the influence of a NAD^+ booster in cells when compared to control non treated cells.

4.1.1.1 *Sensitivity*

Next, it is tested if the NAD^+ measurement method is sensitive enough to calculate a half maximal effective concentration (EC_{50}). This concentration induces a 50 % response between the minimum and maximum response of a sigmoidal activity curve after a certain time of exposure to the compound. This variable is commonly used as a measure of a drug's potency.

The NAD^+ levels are measured on a TSQ™ Triple Quadrupole LC-MS and the results are displayed in **Figure 12**.

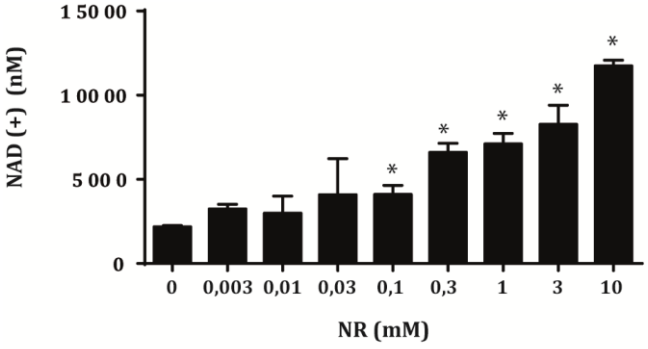

Figure 12: Intracellular NAD^+ levels in AML 12 after 24h treatment increases significantly according to the NR concentration.

Figure 12 displays the level of NAD^+ (n) measured in the cells (AML-12) after a 24 h exposure of NR at a concentration of 0: 0,003; 0,01; 0,03; 0,1; 0,3; 1; 3 and 10 mM. An asterisk (*) represents the significance of the increase of NAD^+ calculated by the unpaired t-test. It is observed that starting from a treatment with 0,1 mM NR the intracellular level of NAD^+ increases significantly corresponding to the dose of NR.

The logarithm of the NR concentration is plotted against the percentage of efficacy, relative to the highest amount of NAD^+ at 10 mM NR in **Figure 13.** The EC_{50} value is calculated using a nonlinear regression. The EC_{50} is 0,63 mM. From these results it is derived that the NAD^+ quantification method is enough sensitive to determine an EC_{50}. A 24 h treatment of 0,63 mM NR induces a 50 % response of increasing NAD^+ level in AML12.

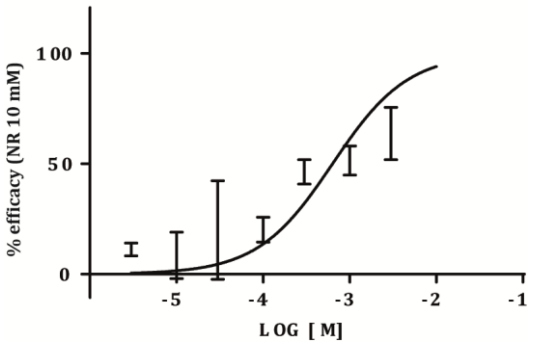

Figure 13: Nonlinear regression is applied on the percentage of efficacy, relative to the highest amount of NAD^+ at 10 mM plotted against the logarithm of the NR concentration. The EC_{50} represents the NR concentration that induces a NAD^+ boost of 50%.

4.1.2 Negative validation

Hydrogen peroxide (H_2O_2) is an inducer of oxidative cell damage. After H_2O_2 exposure of cells, PARPs will be activated and the cells will consume NAD^+. To validate if we can detect a decrease of the NAD^+ pool due to an activation of a NAD^+ consuming enzyme, AML-12 cells have been treated during 1h with H_2O_2 at 500 µM.

As presented in the **Figure 14** we can detect a significant decrease of the NAD^+ level after the H2O2 treatment which confirms the validity of our measurement method *in vitro*.

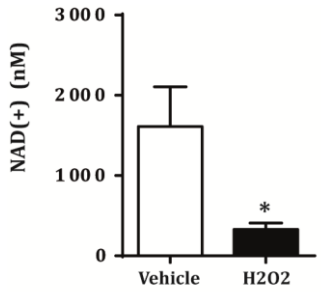

Figure 14: NAD^+ levels after 1h H_2O_2 treatment in AML 12 decrease. H_2O_2 activates NAD^+ consuming PARP enzymes.

4.2 *In vivo* validation of the NAD^+ measurement

4.2.1 Sensitivity

As this NAD^+ measurement method needs to be developed to work in mice samples obtained from the mice BXD population, we had to validate the sensitivity of the method *in vivo.* C57BL/6J mice have been treated during 4 weeks with NR (400mg/kg of body weight) supplemented in the diet. The NAD^+ levels are measured in the liver of these mice. As presented in the **Figure 15** we can detect a significant increase of the NAD^+ level after the NR treatment.

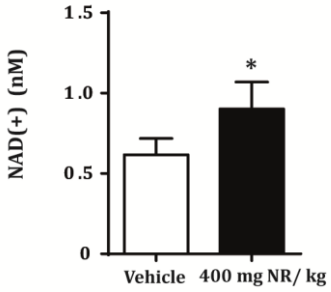

Figure 15: NAD^+ levels in liver of C57BL/6J mice increase after a NR supplemented diet in comparison to a non-treated control.

From these results, it is concluded that both the extraction and measurement method are suitable, allowing us to detect a significant difference in NAD^+ levels in NR treated mice.

4.2.2 Variation

To be able to compare the NAD^+ levels between the different BXD strains, it is necessary to develop a protocol introducing minimal variation. In order to test and validate the best way of normalization, 16 pieces of liver from the same C57BL/6J mice were collected. The results from this experiment are normalized to tissue weight (TW) **(Table 1)**, protein amount **(Table 2)** and the internal standard 2-chloro-adenosine **(Table 3)**. The precision of the method is expressed by the coefficient of variation (CV) **(Table 4** and **Figure 16)**.

4.2.2.1 *Normalization to tissue weight*

Table 1: Normalization NAD^+ level to tissue weight

ID	Mass (mg)	NAD^+ (nM)	Volume of extract (µl)	mol of NAD^+	pmol of NAD^+	pmol of NAD^+/mg tissue
~~1~~	~~NF~~	~~NF~~	NF	NF	NF	NF
2	30,9	44027	500	2,20E-08	22013	712,41
3	23,1	26948	500	1,35E-08	13474	583,28
4	23,7	26104	500	1,31E-08	13052	550,71
5	23,8	25856	500	1,29E-08	12928	543,19
6	20,4	22539	500	1,13E-08	11270	552,44
7	24	42552	500	2,13E-08	21276	886,50
8	24,5	27671	500	1,38E-08	13835	564,71
9	25,6	32812	500	1,64E-08	16406	640,86
10	30,2	35750	500	1,79E-08	17875	591,89
11	23,8	26786	500	1,34E-08	13393	562,74
12	23,5	28486	500	1,42E-08	14243	606,09
13	24	29628	500	1,48E-08	14814	617,25
14	22,5	22428	500	1,12E-08	11214	498,40
15	29,6	30135	500	1,51E-08	15068	509,03
16	26,8	43068	500	2,15E-08	21534	803,51

4.2.2.2 *Normalization to protein amount*

Table 2: Normalization NAD^+ levels to protein amount

ID	Mass (mg)	NAD^+ (nM)	Volume of extract (µl)	mol of NAD^+	pmol of NAD^+	Volume of prot (µl)	prot concentration (µg/µl)	total amount of prot. (µg)	pmol of NAD^+/µg of protein
~~1~~	~~NF~~	~~NF~~	NF	NF	NF	NF	NF	NF	NF
2	30,9	44027	500	2,20E-08	22013	300	3,90	1170	18,81
3	23,1	26948	500	1,35E-08	13474	300	3,24	973	13,85
4	23,7	26104	500	1,31E-08	13052	300	2,88	865	15,09
5	23,8	25856	500	1,29E-08	12928	300	3,73	1120	11,54
6	20,4	22539	500	1,13E-08	11270	300	2,60	781	14,42
7	24	42552	500	2,13E-08	21276	300	3,21	963	22,10
8	24,5	27671	500	1,38E-08	13835	300	3,34	1001	13,83
9	25,6	32812	500	1,64E-08	16406	300	4,02	1206	13,60
10	30,2	35750	500	1,79E-08	17875	300	3,85	1156	15,46
11	23,8	26786	500	1,34E-08	13393	300	2,96	887	15,10
12	23,5	28486	500	1,42E-08	14243	300	3,19	957	14,88
13	24	29628	500	1,48E-08	14814	300	3,25	976	15,17
14	22,5	22428	500	1,12E-08	11214	300	3,02	905	12,39
15	29,6	30135	500	1,51E-08	15068	300	3,53	1059	14,23
16	26,8	43068	500	2,15E-08	21534	300	3,83	1148	18,75

4.2.2.3 *Normalization to internal standard (IS)*

Table 3: Normalization of NAD^+ levels to tissue weight and corrected to the internal standard

ID	IS init. (µM)	IS final (µM)	Efficacy of extraction	NAD^+ (pmol/mg tissue)	NAD^+ (pmol/mg tissue) ext. eff. norm.
2	24,66	0,82	0,033	712,41	21475
3	24,66	0,98	0,040	583,28	14662
4	24,66	1,03	0,042	550,71	13233
5	24,66	1,14	0,046	543,19	11758
6	24,66	1,31	0,053	552,44	10365
7	24,66	1,26	0,051	886,50	17314
8	24,66	1,31	0,053	564,71	10661
9	24,66	1,30	0,053	640,86	12197
10	24,66	1,43	0,058	591,89	10242
11	24,66	1,45	0,059	562,74	9546,66
12	24,66	1,34	0,054	606,09	11126
13	24,66	1,56	0,063	617,25	9782
14	24,66	1,41	0,057	498,41	8713
15	24,66	1,32	0,053	509,04	9534
16	24,66	1,20	0,049	803,52	16444

The C57BL/6J liver samples are extracted in a mix of 17,5 ml of $HLCO_4$ and 0,750 ml of 2-chloro-adenosine at 600 µM. Thus the concentration of internal standard in each extract is 24,66 µM. The remaining concentration IS after extraction is measured by MS. The ratio between both represents the efficacy of the method. The exact amount of NAD^+ is recalculated at an efficacy of 100%. (init. = initial; ext.eff. norm. = extraction efficacy normalized)

4.2.2.4 *Coefficient of variation*

Table 4: NAD^+ levels in C57BL/6J liver normalized to TW, protein amount and internal standard

No.	TW	Protein amount	IS
3	583,28	13,85	14662,25
4	550,71	15,09	13232,94
5	543,19	11,54	11757,52
6	552,44	14,42	10365,05
8	564,71	13,83	10661,02
9	640,86	13,60	12196,73
10	591,89	15,46	10241,55
11	562,74	15,10	9546,66
12	606,09	14,88	11125,87
13	617,25	15,17	9781,54
14	498,41	12,39	8713,28
15	509,04	14,23	9534,30
Standard deviation	42,11	1,19	1718,48
Average	573,78	14,12	11116,76
CV	**7,34**	**8,43**	**15,46**

The CV is calculated as the ratio of the standard deviation and the average of the value of NAD^+ in pmol / standardization unit.

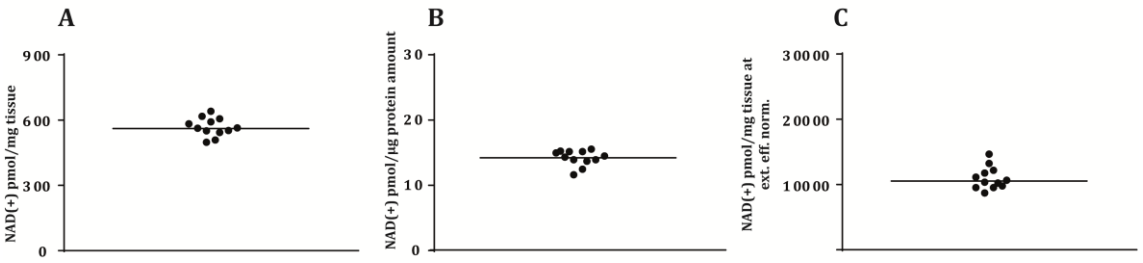

Figure 16: CV of normalization to TW (A), protein amount (B) and internal standard (C)

The goal of this experiment was to compare the variation between various normalization methods. The obtained CV are 7 % (TW), 8 % (protein amount) and 15 % when normalization to TW is corrected to an extraction efficacy of 100 % based on the (IS). Thus, introducing a correction for the IS induced more variation. This can be due to the fact that the solubility of 2-chloro-adenosine in methanol might not be complete. This will result in the calculation of a lower extraction efficacy in each sample. Secondly, the different steps in the extraction method might influence the stability of the compound. In the future it might be useful to compare 2-chloro-adenosine to other internal standards described in literature.

These results prove that by using the described extraction method and LC-MS/MS allows us to compare NAD^+ levels in the same liver. The normalization to TW and protein induces a similar variation while normalizing to the IS induces more variation. It is concluded that the normalization to TW and protein amount will be used to detect the NAD^+ levels in BXD.

4.3 BXD

54 BXD strains were fed with CD and HFD for 28 weeks. At sacrifice, their livers were collected, snap-frozen and stored at -80°C. NAD^+ was extracted from these tissues and analyzed by LC-MS/MS. The raw data derived from LC-MS/MS analysis were corrected by a batch factor and a NAD^+ standard. These values correct the variation induced by respectively the difference in extraction efficiency between the batches and the LC-MS/MS. Next, the outliers were removed with a boxplot analysis.

Figure 17 shows the distribution of the NAD^+ levels in the strains on CD and HFD. The strains on HFD are ranked lower in comparison with the strains on CD. This supports the validity of our data. The BXD parental strain of C57BL/6J was used as internal control strain. Comparison between both diets show the NAD^+ levels in C57BL/6J mice are lowered under HFD. Similar results were obtained in previous research (Gariani, K. et al., 2016) and validates our work.

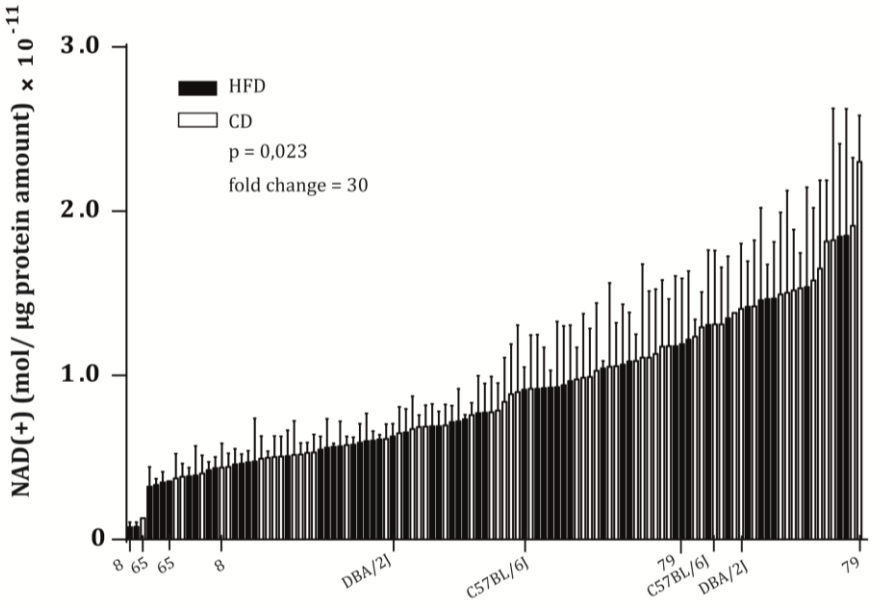

Figure 17: Distribution of NAD^+ levels in the BXD on CD and HFD.

Figure 18 shows the correlation of the NAD^+ levels between the BXD strains on CD and HFD. The p-value of 0.35 is higher than the initially set p-value of 0.05 and the correlation coefficient r is -0,13. Hence it is concluded that the linear relationship is negative and very weak, which means there is no direct correlation between the data sets on CD and HFD.

It is concluded that there are no strong genetic factors responsible for the NAD+ regulation.

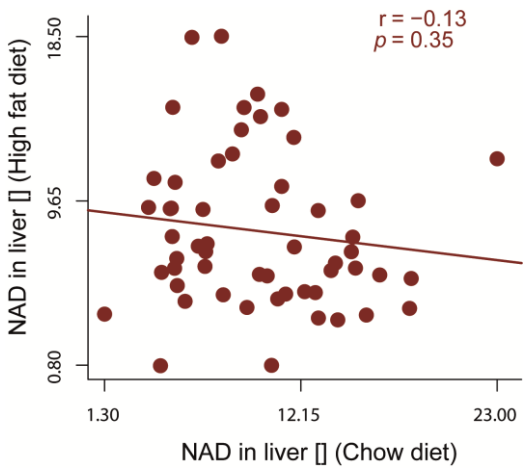

Figure 18: Correlation analysis between the strains on chow and high fat diet.

In **Figure 19** the different QTLs are mapped for strains on CD. The likelihood ratio statistic (LRS) on the y-axis, a statistical value, is plotted against the different chromosomes for NAD^+ levels in CD. The minimal LRS for a statistical significant QTL is set at 17. The peaks crossing the likelihood ratio statistic (LRS) of 10 are suggestive loci that may contain genes responsible for the modulation of the intracellular NAD^+ levels. **Figure 19** shows that two suggestive QTLs are located in chromosome 4 and 6 in strains under CD.

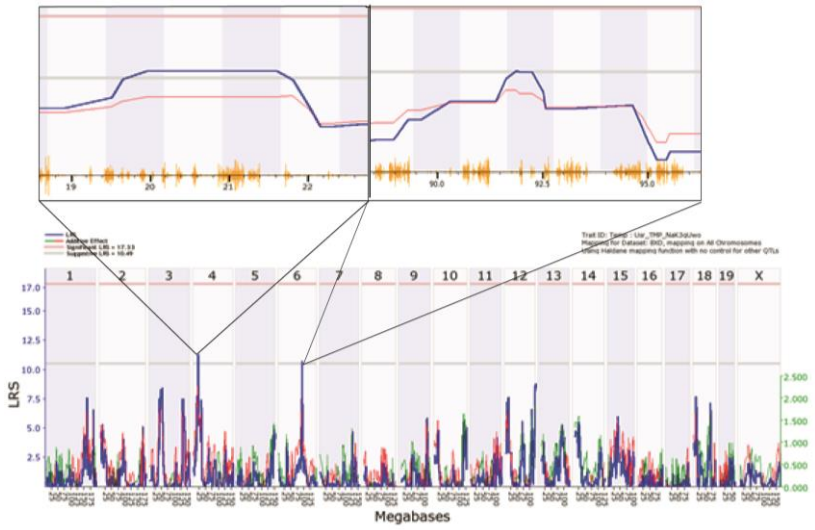

Figure 19: QTL mapping in CD showing all the chromosomes. The enlargements show the QTL on the specific chromosomes 4 and 6.

The region in chromosome 4 is situated between 19,2 and 22 megabases (Mb) and in chromosome 6 between 91,7 and 92,3 Mb. Combined there are 29 genes under these suggestive QTLs and they merit further evaluation for a potential role in the regulation of liver NAD^+ levels in mice fed CD.

Figure 20 presents the suggestive QTLs in strains under HFD are located in chromosome 4, 15 and 17.

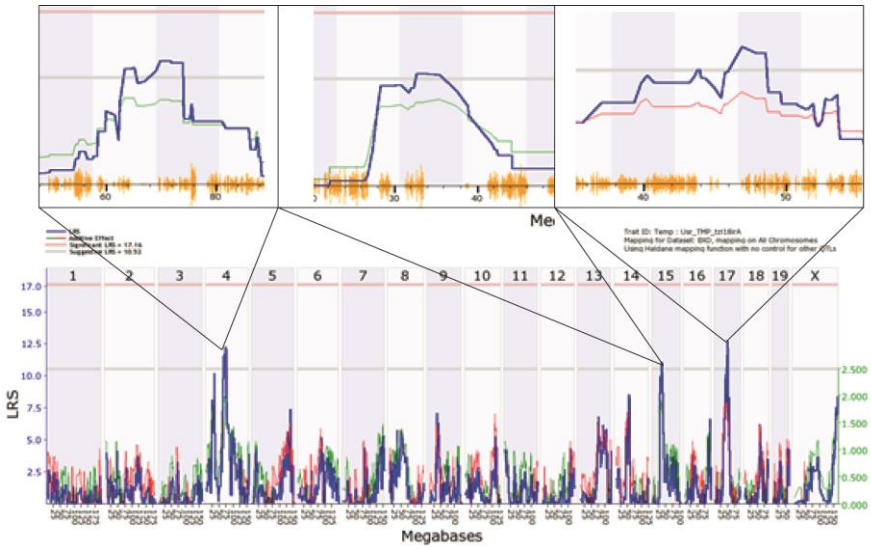

Figure 20: QTL mapping in HFD showing all the chromosomes. The enlargements show the QTL on the specific chromosomes 4, 15 and 17.

The region on chromosome 4 is situated between 62 and 75 Mb and on chromosome 15 between 32 and 36 Mb. The QTLs on chromosome 17 are located between 45,5 and 49 Mb. 200 candidate genes are located under these 3 QTLs combined. These regions would be worth to be explored for a potential role in NAD^+ regulation.

5 Discussion

The regulation of NAD^+ metabolism via pharmacological compounds such as nicotinamide riboside (NR) has already proven its ability to enhance metabolic function through activation of the NAD^+ / sirtuin pathway. My study aimed to determine the Quantitative Trait Loci (QTL) and potential Quantitative Trait Genes (QTGs) responsible for the regulation of NAD^+ levels in the BXD mice population using forward genetics. Identifying such genes would open perspectives to develop drugs against them to modulate NAD^+ levels and to potentially use them in metabolic diseases.

We developed and validated first a reliable NAD^+ extraction and LC-MS/MS measurement method. We are able to detect a significant increase and decrease of NAD^+ levels caused by respective treatments with a NAD^+ booster (NR) and the PARP activator (H_2O_2) in mouse AML12 hepatocytes. Next the sensitivity of the method was validated *in vitro* by performing an EC_{50} calculation for NR. *In vivo* the method was validated by reliably measuring the increase in NAD^+ levels seen in C57BL/6J mice treated with NR. Furthermore, we performed several tests on normalization methods for the NAD^+ measurement. The normalization of NAD^+ levels to tissue weight and protein amount showed a similar coefficient of variation. Both were used to normalize the BXD data.

We then measured NAD^+ levels in 437 liver samples from 54 different strains of the BXD GRP to map 2 suggestive QTLs under CD and 3 suggestive QTLs in mice fed HFD. These loci are likely contributing to determining liver NAD^+ levels. Of note, the suggested QTLs responsible for NAD^+ differ in mice fed on CD and HFD. On CD these regions were located on chromosome 4 between 19,2 and 22 Mb and on chromosome 6 between 91,7 and 92,3 Mb, with 29 underlying genes under both loci combined as potential NAD^+ regulators on under CD. In BXD strains under HFD, QTLs are situated on chromosome 4, 15 and 17. These areas can be specified to 62-75 Mb (chr4), 32-36 Mb (chr15) and 45,5-49 Mb (chr17). These three suggestive QTLs combined encompass ~200 candidate QTGs with a potential role in NAD^+ regulation on HFD. We have observed no correlation between the strains on both diets, which makes us conclude that there is no strong genetic effect on the regulation of the NAD^+ levels. In the future the genetic and environmental factors that contribute to determining NAD^+ levels can be modeled using additional statistical tools. A logical next step would be to detect the genetic interactions and uncover the biological pathways that are uncovered by these QTLs.

Future work includes correlation analysis with phenotypic, microarray, proteomics data and important NAD^+ metabolism genes. Such type of analysis will allow us to validate the already known correlations and networks and it would support the identification of new pathways, which could modulate NAD^+ levels.

References

Andreux, P. A., Williams, E. G., Koutnikova, H., Houtkooper, R. H., Champy, M. F., & Henry, H., et al. (2012). Systems genetics of metabolism: the use of the BXD murine reference panel for multiscalar integration of traits. *Cell, 150*(6), 1287-1299.

Balentine, J., & Conrad, M. (2016). *Obesity.* Retrieved June 17, from http://www.medicinenet.com/obesity_weight_loss/page3.htm

Barbosa, M. T. P., Soares, S. M., Novak, C. M., Sinclair, D., Levine, J. A., & Aksoy, P., et al. (2007). The enzyme CD38 (a NAD glycohydrolase, EC 3.2.2.5) is necessary for the development of diet-induced obesity. *FASEB journal : official publication of the Federation of American Societies for Experimental Biology, 21*(13), 3629-3639.

Bechmann, L. P., Hannivoort, R. A., Gerken, G., Hotamisligil, G. S., Trauner, M., & Canbay, A., et al. (2012). The interaction of hepatic lipid and glucose metabolism in liver diseases. *J Hepatol, 56*(4), 952-964.

Camacho-Pereira, J., Tarragó, M. G., Chini, C. C. S., Nin, V., Escande, C., & Warner, G. M., et al. (2016). CD38 Dictates Age-Related NAD Decline and Mitochondrial Dysfunction through an SIRT3-Dependent Mechanism. *Cell Metab, 23*(6), 1127-1139.

Cantó, C., & Auwerx, J. (2012). Targeting sirtuin 1 to improve metabolism: all you need is NAD(+)? *Pharmacol Rev, 64*(1), 166-187.

Cantó, C., Gerhart-Hines, Z., Feige, J. N., Lagouge, M., Noriega, L., & Milne, J. C., et al. (2009). AMPK regulates energy expenditure by modulating NAD+ metabolism and SIRT1 activity. *Nature, 458*(7241), 1056-1060.

Cantó, C., Houtkooper, R. H., Pirinen, E., Youn, D. Y., Oosterveer, M. H., & Cen, Y., et al. (2012). The NAD(+) precursor nicotinamide riboside enhances oxidative metabolism and protects against high-fat diet-induced obesity. *Cell Metab, 15*(6), 838-847.

Cantó, C., Jiang, L. Q., Deshmukh, A. S., Mataki, C., Coste, A., & Lagouge, M., et al. (2010). Interdependence of AMPK and SIRT1 for metabolic adaptation to fasting and exercise in skeletal muscle. *Cell Metab, 11*(3), 213-219.

Cantó, C., Menzies, K. J., & Auwerx, J. (2015). NAD(+) Metabolism and the Control of Energy Homeostasis: A Balancing Act between Mitochondria and the Nucleus. *Cell Metab, 22*(1), 31-53.

CHAMBON, P., WEILL, J. D., & MANDEL, P. (1963). Nicotinamide mononucleotide activation of new DNA-dependent polyadenylic acid synthesizing nuclear enzyme. *Biochem Biophys Res Commun, 11*, 39-43.

Gariani, K., Menzies, K. J., Ryu, D., Wegner, C. J., Wang, X., & Ropelle, E. R., et al. (2016). Eliciting the mitochondrial unfolded protein response by nicotinamide adenine dinucleotide repletion reverses fatty liver disease in mice. *Hepatology, 63*(4), 1190-1204.

GeneNetwork (2016). *What is GeneNetwork.* Retrieved 15 June 2015, from http://www.genenetwork.org/home.html

Gregor, M. F., & Hotamisligil, G. S. (2011). Inflammatory mechanisms in obesity. *Annu Rev Immunol, 29*, 415-445.

Harms, M., & Seale, P. (2013). Brown and beige fat: development, function and therapeutic potential. *Nat Med, 19*(10), 1252-1263.

Harvard T.H. Chan (2016). *Weight Problems Take a Hefty Toll on Body and Mind.* Retrieved June 2, from https://www.hsph.harvard.edu/obesity-prevention-source/obesity-consequences/health-effects/

Houtkooper, R. H., & Auwerx, J. (2012). Exploring the therapeutic space around NAD+. *J Cell Biol, 199*(2), 205-209.

Houtkooper, R. H., Cantó, C., Wanders, R. J., & Auwerx, J. (2010). The secret life of NAD+: an old metabolite controlling new metabolic signaling pathways. *Endocr Rev, 31*(2), 194-223.

Houtkooper, R. H., Pirinen, E., & Auwerx, J. (2012). Sirtuins as regulators of metabolism and healthspan. *Nat Rev Mol Cell Biol, 13*(4), 225-238.

Imai, S. I. (2009). The NAD World: a new systemic regulatory network for metabolism and aging--Sirt1, systemic NAD biosynthesis, and their importance. *Cell Biochem Biophys, 53*(2), 65-74.

Kim, H. J., Kim, J. H., Noh, S., Hur, H. J., Sung, M. J., & Hwang, J. T., et al. (2011). Metabolomic analysis of livers and serum from high-fat diet induced obese mice. *J Proteome Res, 10*(2), 722-731.

Kinesis (2016). *Mass spectrometer detectors.* Retrieved August 19 2016, from http://kinesis.co.uk/media/wysiwyg/knowledebase/pdf/Mass_Spectrometer_Detectors.pdf

Labcompare (2009). *Triple Quadrupole Mass Spectrometer (QqQ MS).* Retrieved August 19 2016, from http://www.labcompare.com/Mass-Spectrometry/131-Triple-Quadrupole-Mass-Spectrometer-QqQ-MS/

Manco, M., Calvani, M., & Mingrone, G. (2004). Effects of dietary fatty acids on insulin sensitivity and secretion. *Diabetes Obes Metab, 6*(6), 402-413.

Mouchiroud, L., Houtkooper, R. H., & Auwerx, J. (2013). NAD^+ metabolism: a therapeutic target for age-related metabolic disease. *Crit Rev Biochem Mol Biol, 48*(4), 397-408.

Mouchiroud, L., Houtkooper, R. H., Moullan, N., Katsyuba, E., Ryu, D., & Cantó, C., et al. (2013). The NAD(+)/Sirtuin Pathway Modulates Longevity through Activation of Mitochondrial UPR and FOXO Signaling. *Cell, 154*(2), 430-441.

Patil, V., Tathe, R., Devdhe, S., Angadi, S., & Kale, S. (2011). Ultra performance liquid chromatography: a review. *International research journal of pharmacy, 2*(6), 39-44.

Peirce, J. L., Lu, L., Gu, J., Silver, L. M., & Williams, R. W. (2004). A new set of BXD recombinant inbred lines from advanced intercross populations in mice. *BMC Genet, 5*, 7.

Pfluger, P. T., Herranz, D., Velasco-Miguel, S., Serrano, M., & Tschöp, M. H. (2008). Sirt1 protects against high-fat diet-induced metabolic damage. *Proc Natl Acad Sci U S A, 105*(28), 9793-9798.

Richard A Harvey (Ph D), Harvey, R. A., & Ferrier, D. R. (2011). *Biochemistry.* Lippincott Williams & Wilkins.

Srivastava, S. (2016). Emerging therapeutic roles for NAD(+) metabolism in mitochondrial and age-related disorders. *Clinical and translational medicine, 5*(1), 25.

Suman, S., Rajni, B., & Gill, N. (2014). Ultra Performance Liquid chromatography: An Introduction. *Journal of Drug discovery and therapeutics, 22*(2), 12-17.

ThermoFisher (2015). *TSQ Quantum™ Access MAX Triple Quadrupole Mass Spectrometer.* Retrieved June 17, from https://www.thermofisher.com/order/catalog/product/IQLAAEGAAXFAGBMAWU

True Life Research (2016). *Nicotinamide Adenine Dinucleotide (NAD) 99% CAS 53-84-9.* Retrieved July 30, from https://teamtlr.com/anti-aginglongevity-research/73-nicotinamide-adenine-dinucleotide-nad-99.html

University of Pittsburgh (2016). *Mass spectrometry introduction.* Retrieved August 18 2016, from http://www.chem.pitt.edu/facilities/mass-spectrometry/mass-spectrometry-introduction

Verdin, E. (2015). NAD^+ in aging, metabolism, and neurodegeneration. *Science, 350*(6265), 1208-1213.

Verduin, P., Agarwal, S., & Waltman, S. (2005). Solutions to obesity: perspectives from the food industry. *Am J Clin Nutr, 82*(1 Suppl), 259S-261S.

Whitbread, D. (2016). *Top 10 Foods highest in tryptophan.* Retrieved June 4 2016, from https://www.healthaliciousness.com/articles/high-tryptophan-foods.php

World Health Organization (WHO) (2016). *Background: the global burden of chronic.* Retrieved 13/08/2016, from http://www.who.int/nutrition/topics/2_background/en/

World Health Organization (2016). *Obesity and overweight.* Retrieved June 17 2016, from http://www.who.int/mediacentre/factsheets/fs311/en/

Yang, B., & Kirchmaier, A. L. (2006). Bypassing the catalytic activity of SIR2 for SIR protein spreading in Saccharomyces cerevisiae. *Mol Biol Cell, 17*(12), 5287-5297.

Auteursrechtelijke overeenkomst

Ik/wij verlenen het wereldwijde auteursrecht voor de ingediende eindverhandeling:
Genetic and environmental impact on NAD⁺ levels

Richting: **master in de industriële wetenschappen: biochemie**
Jaar: **2016**

in alle mogelijke mediaformaten, - bestaande en in de toekomst te ontwikkelen - , aan de Universiteit Hasselt.

Niet tegenstaand deze toekenning van het auteursrecht aan de Universiteit Hasselt behoud ik als auteur het recht om de eindverhandeling, - in zijn geheel of gedeeltelijk -, vrij te reproduceren, (her)publiceren of distribueren zonder de toelating te moeten verkrijgen van de Universiteit Hasselt.

Ik bevestig dat de eindverhandeling mijn origineel werk is, en dat ik het recht heb om de rechten te verlenen die in deze overeenkomst worden beschreven. Ik verklaar tevens dat de eindverhandeling, naar mijn weten, het auteursrecht van anderen niet overtreedt.

Ik verklaar tevens dat ik voor het materiaal in de eindverhandeling dat beschermd wordt door het auteursrecht, de nodige toelatingen heb verkregen zodat ik deze ook aan de Universiteit Hasselt kan overdragen en dat dit duidelijk in de tekst en inhoud van de eindverhandeling werd genotificeerd.

Universiteit Hasselt zal mij als auteur(s) van de eindverhandeling identificeren en zal geen wijzigingen aanbrengen aan de eindverhandeling, uitgezonderd deze toegelaten door deze overeenkomst.

Voor akkoord,

Vrijens, Lisa

Datum: **19/08/2016**